Nanoscale

High Solid-State Photoluminescence Quantum Yield of Carbon-Dot-Derived Molecular Fluorophores for Light-Emitting Devices

Journal:	*Nanoscale*
Manuscript ID	NR-ART-04-2024-001672
Article Type:	Paper
Date Submitted by the Author:	16-Apr-2024
Complete List of Authors:	Javed, Nasir; Rutgers University Pacheco, Haydee; Rutgers University Sreekumar, Sneha; Rutgers University Chong, Jinyu; Rutgers University Cheng, Zhongkai; Rutgers University O'Carroll, Deirdre; Rutgers University

ARTICLE

High Solid-State Photoluminescence Quantum Yield of Carbon-Dot-Derived Molecular Fluorophores for Light-Emitting Devices†

Received 00th January 20xx,
Accepted 00th January 20xx

DOI: 10.1039/x0xx00000x

Nasir Javed,*[ab] Haydee Pacheco,[a] Sneha Sreekumar,[c] Jinyu Chong,[c] Zhongkai Cheng [c] and Deirdre O'Carroll*[ac]

Several recent studies of carbon dots (CDs) synthesized by bottom-up methods at mild conditions have reported the presence of organic molecular fluorophores in CD dispersions. These fluorophores have a tendency to aggregate, and their properties strongly depend on whether they are present in the form of discrete molecules or aggregates. The aggregation becomes more prominent in the solid state, which motivates the study of the properties of the fluorophores associated with CDs in the solid state. Here, we report the solid-state characterization of N4,N11-dimethyldibenzo[a,h]phenazine-4,11-diamine (BPD) - a molecular fluorophore that forms CDs. Discrete BPD molecules show excitation-wavelength-independent photoluminescence (PL) emission in the green wavelength region at ~520 nm. However, additional blue PL is also observed due to aggregation, making the PL emission significantly broad. For detailed studies, BPD is mixed in different solid matrices, and it is observed that the PL quantum yield (PLQY) of BPD films strongly depends on the concentration of BPD in the solid matrices. Increasing the concentration of BPD results in a considerable decrease in the PLQY. The PLQY of the films with an optimum concentration of BPD is 75.9 % and 40.2 % in polymethyl methacrylate and polystyrene, respectively. At higher concentrations, these PLQY values decrease to ~11 %. The significant decrease in the PLQY is ascribed to reabsorption and nonradiative exciton decay that is facilitated by BPD aggregation at higher concentrations. Finally, light-emitting devices (LEDs) were fabricated with almost pure white emission color, having CIE (International Commission on Illumination) coordinates of (0.35, 0.37) using BPD in the color-converting layer of blue-pumped LEDs. The device shows a luminous efficiency 3.8 lm/W and luminance of 43,331 cd/m^2.

Introduction

The desire to achieve efficient and bright photoluminescence (PL) from CDs has driven researchers to explore bottom-up synthesis methods.[1-4] Typically, during a bottom-up synthesis, small molecular precursors are subjected to heat treatment to assist carbonization and formation of carbon-based particles.[5, 6] However, when the reaction is carried out at mild conditions, complete carbonization is not achieved.[7] Instead, several intermediate species form in addition to carbonized particles. Several recent studies of CDs synthesized by bottom-up methods at mild conditions have reported the presence of organic molecular fluorophores in the CD dispersions.[8-11] These fluorophores can be present on the surface of the CDs, freely floating in the dispersion, or even form a polymer network to construct a spherical particle with characteristics similar to CDs.[11-13] These fluorophores have a tendency to aggregate, and their properties strongly depend on whether they are present in the form of discrete molecules or aggregates.[14, 15] Therefore, studying their optical properties is difficult due to the complex interactions between the molecules and their aggregates. This aggregation becomes more prominent in the solid state, which motivates the study of the properties of fluorophores associated with CDs in the solid state.

Applications of high PL quantum yield (PLQY) CDs or associated fluorophores in optoelectronics rely on their optical properties in the solid state.[16-20] Yet, the PLQY is mostly measured in solutions. Although a few studies report the PLQY of the CDs or fluorophores in the solid state,[21-24] there are very few studies that thoroughly investigate the optical properties, including concentration dependence and reabsorption by CDs or fluorophores in the solid state. Ren et al. studied the optical properties of CDs/fluorophores in polystyrene (PS), polymethyl methacrylate (PMMA), and four different ormosil (organically modified silica) gel glasses.[25] They reported a strong redshift in the PL emission color of CDs with the increasing polarity of the solid matrix. Wang et al. studied the PL emission from CD-based films in a transmission geometry by placing the excitation source and detectors on the opposite sides of the films. They noted a strong thickness-dependent redshift in the PL emission color that was attributed to the reabsorption.[26] Meng et al. reported a shift in fluorescence emission wavelengths from CDs depending on their concentration in solution.[27] In the solid state or at higher concentrations in

---

[a] *Department of Materials Science and Engineering, Rutgers, The State University of New Jersey, 607 Taylor Road, Piscataway, NJ 08854, USA.*
[b] *Faculty of Engineering Sciences, Ghulam Ishaq Khan Institute of Engineering Sciences and Technology, Topi, 23460, Khyber Pakhtunkhwa, Pakistan.*
[c] *Department of Chemistry and Chemical Biology, Rutgers, The State University of New Jersey, 123 Bevier Road, Piscataway, NJ 08854, USA*

† Electronic Supplementary Information (ESI) available: See DOI: 10.1039/x0xx00000x

dispersions, there can be interactions between fluorophores or between fluorophores and CDs (carbon core) that can have several consequences, including intermolecular charge transfer and the formation of nonradiative decay pathways.[28]. These phenomena can limit the PLQY or affect the PL emission color. Therefore, a comprehensive characterization of the fluorophores in the solid state is needed to control better and optimize devices made from CDs.

In this study, we report the detailed solid-state characterization of N^4,N^{11}-dimethyldibenzo[a,h]phenazine-4,11-diamine (BPD) – a molecular fluorophore that forms CDs.[11] Synthesis was carried out by a previously reported solvothermal treatment of citric acid and 1,5-diaminonaphthalene in methanol. This reaction yields spherical CD-like particles which can be dissolved/disintegrated in organic solvents to collect BPD molecules. BPD shows excitation-wavelength-independent PL emission in the green wavelength region at ~520 nm. For the solid-state study, BPD is mixed in different solid matrices (optical epoxy, PMMA, PS, and poly(9-vinylcarbazole) (PVK)), and films are prepared. It is observed that the PLQY of BPD in solid matrices strongly depends on the concentration (wt. %) of BPD. The PLQY of the films with optimum concentration of BPD is 75.9 % and 40.2 % in PMMA and PS, respectively. Increasing the concentration of BPD results in a considerable decrease in its PLQY. The significant decrease in the PLQY is ascribed to reabsorption and nonradiative exciton decay that is facilitated by aggregation at higher concentrations. In addition to high PLQY values at optimum concentration, the BPD films show broadband, white color PL emission. The broad PL emission and high PLQY of the films were exploited for the fabrication of optically driven white light-emitting devices (LEDs). LEDs with almost pure white emission color having CIE (International Commission on Illumination) coordinates of (0.35, 0.37) are fabricated using BPD in the color converting layer (CCL) of blue-pumped LEDs. The device shows a luminous efficiency of 3.8 lm/W (luminance 43,331 cd/m^2).

Experimental

Material

Citric acid (≥ 99.5%), polystyrene (Mw: 35,000), poly(9-vinylcarbazole) (Mn: 25,000-50,000), chlorobenzene (ACS regent ≥ 99.5 %), and dichloromethane (anhydrous ≥ 99.8%), were purchased from Sigma-Aldrich. Methanol (certified ACS ≥ 99.8%) was acquired from Fisher Chemical. 1,5-diaminonaphthalene (> 98.0%) was acquired from Tokyo Chemical Industry Co., Ltd. Polymethyl methacrylate (Mw: 35,000) was purchased from Acros Organics Milli-Q 18.2 MΩ cm deionized water was used in this study. All purchased materials and chemicals were used without further purification.

Synthesis and Fabrication

Carbon dots were synthesized using a previously reported solvothermal method.[11] Briefly, 10 mg of citric acid and 20 mg of 1,5-diaminonaphthalene were dissolved in 10 mL of methanol. The solution was transferred to a 20 mL Teflon-lined, stainless-steel, hydrothermal autoclave and then heated at 200 °C for 5 hr. After heat treatment, the dark brown solution was diluted with deionized water and dialyzed for two days using a regenerated cellulose dialysis membrane having a molecular weight cutoff of 3.5 kDa (Spectrum Laboratories Inc., manufacturer part number: 132725). The dialysis was carried out in a 1-liter beaker, and the water was changed frequently. After the dialysis, the purified product, which contains spherical carbon dot-like particles, was dried in a rotary evaporator. Discrete N^4,N^{11}-dimethyldibenzo[a,h]phenazine-4,11-diamine molecules and their aggregates were collected by dissolving the particles in dichloromethane.

For solid-state measurements, films of BPD in different polymers were prepared on glass coverslips. First, the coverslips were cleaned sequentially by sonicating them for 15 minutes each in Sparkleen water, deionized water, acetone, and isopropanol. PMMA, PS, and PVK were dissolved in chlorobenzene at 100 mg/mL, and BPD was dissolved in dichloromethane at 1 mg/mL. The polymer and BPD solutions were combined to make a mixture of the required wt.% of BPD in the polymers. The mixtures were then drop-cast on glass coverslips. After drying, the samples were encapsulated by optical epoxy (Norland Optical Adhesive (NOA 63)) and another clean coverslip, and cured under 365 nm UV light for 20 minutes before characterization. For mixing BPD in epoxy, first, the mass of a small quantity of epoxy was measured, and then the required quantity of BPD solution was added and mixed for several minutes. The mixture was left in a vacuum desiccator for 1 hour to remove the solvent and air bubbles. Finally, the mixture was sandwiched between two glass coverslips and cured in UV light for 20 minutes. Optically driven LEDs were fabricated using BPD as a CCL. Two different high-power (10 W) LED chips (Chanzon) with emission wavelengths of 375 nm and 445 nm were selected for the device fabrication. For the CCL, 0.5 wt. % of BPD was mixed in PMMA and epoxy separately. The mixtures were then coated on LED chips and sealed with epoxy and glass coverslip for encapsulation.

Characterization

UV-visible absorption spectra were recorded using a SI Photonics CCD Array UV-vis Spectrometer equipped with deuterium and tungsten lamps for UV and visible light analysis, respectively. For solution samples, quartz cuvettes of 10 mm path length were used to hold the samples. Photoluminescence (PL) emission and excitation were measured on a Horiba Fluorolog-3 spectrofluorometer. The spectrofluorometer was equipped with a 450 W xenon lamp source; a double monochromator was used on the excitation side, and the PL emission was collected through an iHR 320 emission monochromator and a Hamamatsu R928P photomultiplier tube (PMT) detector. Excitation and emission slit widths were set to 3 nm (bandpass) unless otherwise mentioned in the results. Film samples and cuvettes (standard 10 mm square quartz) were held perpendicular to the excitation beam, and the PL emission was collected from the front face of cuvettes/films (i.e., the PL emission signal was detected at 22.5° to the incident light path). Absolute PL quantum yield (PLQY) was measured with a calibrated integrating sphere (F-3018) on the same spectrofluorometer using 340 nm and 375 nm excitation wavelengths (λ_{exc}). Scattered spectra were integrated over the wavelength range from (λ_{exc} – 5 nm) to (λ_{exc} + 5 nm). For λ_{exc} of 340 nm, PL emission was integrated from 380 nm to 700 nm, and for λ_{exc} of 375 nm, PL emission was integrated from 430 nm to 700 nm.

Time-resolved PL measurements were carried out using a PicoQuant lifetime measurement system. The samples were excited with a pulsed 375 nm wavelength laser (pulse duration of 40 ps; repetition rate of 10 MHz) using a PicoQuant picosecond pulsed diode laser (PDL 800-D) through a Zeiss Axio Vert.A1 inverted microscope using a 20 x objective lens. The PL emission was collected using the same objective and focused onto a single-photon-counting detector module (PDM Series, Micro Photon Devices) after passing through a 400 nm long-pass filter. The pulsed excitation laser and detector module were coupled to a time-correlated, single-photon-counting system (TimeHarp 260 PICO, PicoQuant) to acquire PL lifetime decay curves. PL lifetime components were extracted by fitting the PL lifetime decay curves to an exponential tail fit using FluoFit software (PicoQuant). PL images were acquired using a Zeiss Vert.A1 Inverted microscope equipped with a 20 x objective lens. A 120 W mercury vapor short arc lamp (Excelitas Technologies X-Cite Series 120 Q) was used as the excitation source. Illumination and emission were facilitated by a filter cube that has a 365/12 nm bandpass filter on the excitation side and a 397 nm long pass filter on the emission side. Images were recorded using a Zeiss Axiocam 506 color camera. PL spectra at the same illumination condition were also recorded using an ANDOR Shamrock SR-303i imaging spectrograph equipped with an ANDOR Newton CCD detector (Model No. DU940P-BV).

For electroluminescence measurements, power was supplied by a Keithley 2400 SourceMeter (applied voltage: 10 V, compliance current: 1 A), and the emission was measured using a BWTEK Inc. Glacier X thermoelectrically cooled CCD array spectrometer. For the luminance measurements, the power was supplied using the same source meter, and the luminance was measured by a Konica Minolta CS-200 chroma meter. The source meter and chroma meter were controlled and synchronized by LabVIEW software. Luminous efficiency was calculated from the luminance date and using a vertex angle of 140º as given in the LED chips specifications. The color rendering index was calculated using the method described by K. Smet et al. [29]

Results and Discussion

Figure 1: Optical properties of BPD measured in dichloromethane: (a) UV-vis absorbance spectrum and PL excitation spectra measured from PL emission wavelengths of 485 nm and 525 nm. (b) 2D color scaled contour map of PL emission measured using different excitation wavelengths. PL excitation and emission were measured for a solution concentration of 4 μg/mL. (c) Concentration-dependent PLQY of BPD in DCM.

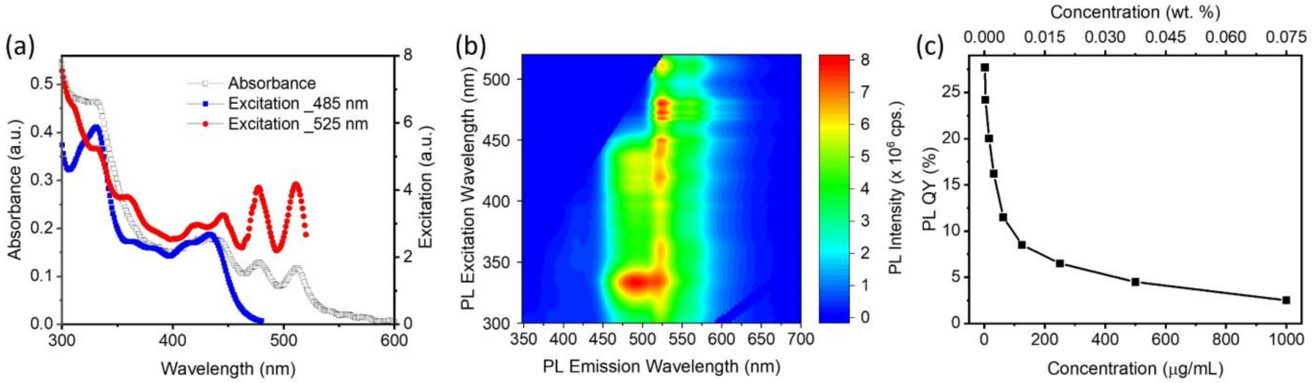

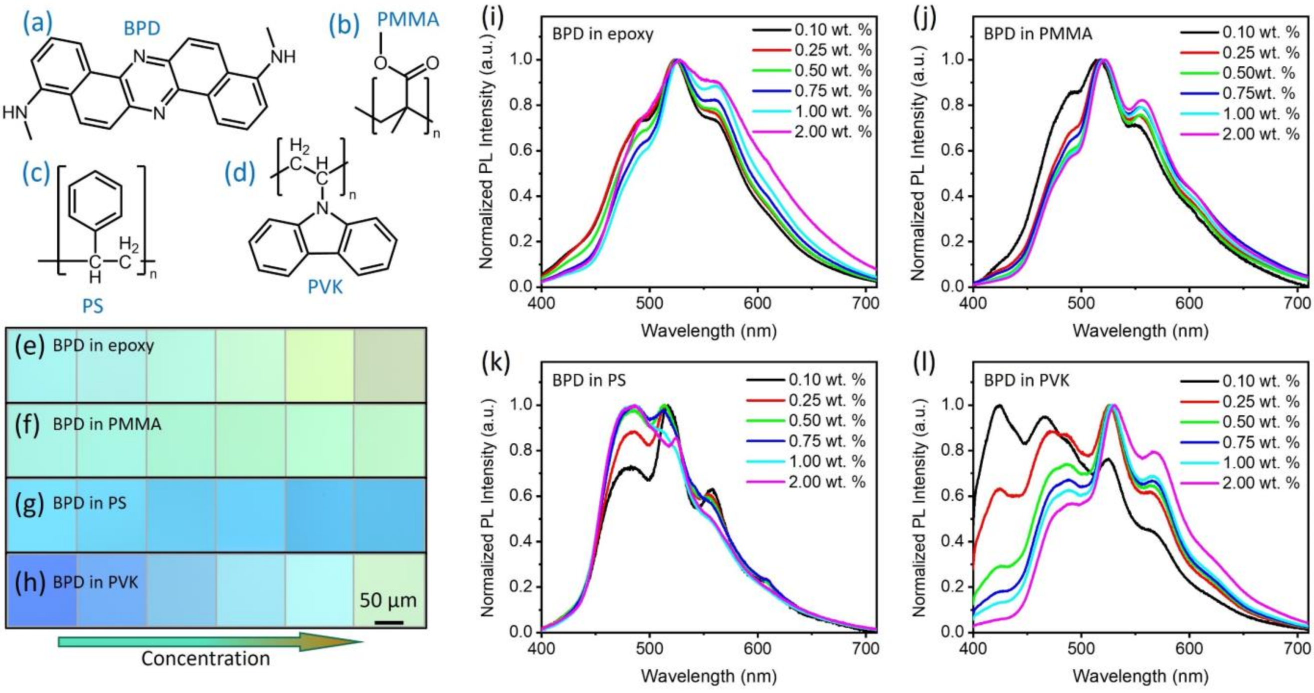

Figure 2: Molecular structure of (a) BPD, (b) PMMA, (c) PS, and (l) PVK. PL images of films of BPD mixed in (e) Epoxy, (f) PMMA, (g) PS, and (h) PVK at different concentration recorded using an excitation wavelength of 365 nm. Concentration from left to right is 0.10, 0.25, 0.50, 0.75, 1.00, and 2.00 wt. %, respectively. PL Emission spectra of BPD mixed in (i) Epoxy, (j) PMMA, (k) PS, and (l) PVK at different concentration recorded using an excitation wavelength of 365 nm.

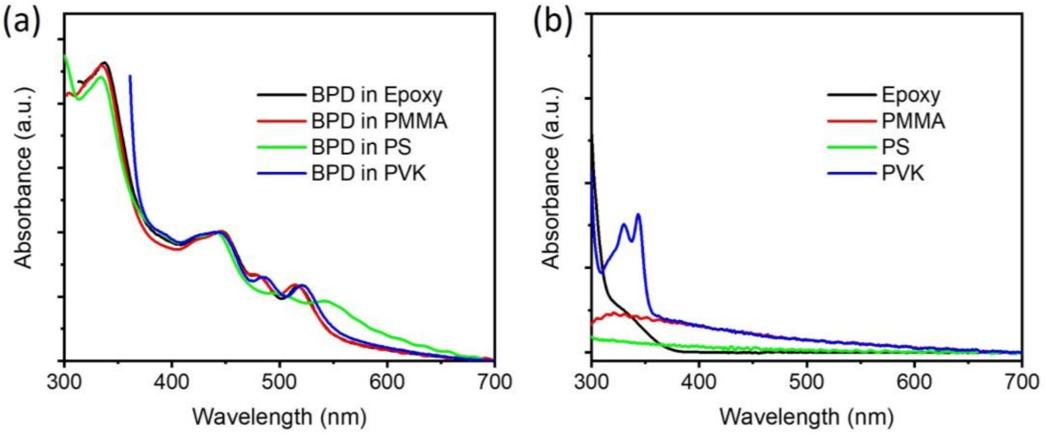

Figure 3 : (a) UV-visible absorbance of BPD, normalized at 440 nm, measured in different polymer matrices at a concentration of 2.0 wt. %. The absorbance spectrum of BPD in PVK (blue line) is clipped below 360 nm due to the strong noise caused by the high absorption by PVK. (b) UV-visible absorbance of pure polymer matrices.

First, we study the optical properties of BPD in the solution state. The absorbance spectrum of BPD in dichloromethane (DCM), as shown in **Figure 1a**, shows a strong UV absorption at 330 nm, in addition to sharp absorption peaks in the visible region at 510 nm, 477 nm, and 445 nm. The absorption peak at 510 nm is due to electronic transition from the highest occupied molecular orbital (HOMO) to the lowest unoccupied molecular orbital (LUMO) of BPD, and the peaks at 477 nm and 445 nm are due to vibronic progression.[11] BPD shows strong photoluminescence (PL) emission centered at 525 nm (Figure 1b) that is associated with the absorption at 510 nm, as depicted by excitation spectra in Figure 1a. However, for short-wavelength excitation, BPD also shows blue PL emission that is mainly excited by excitation into the UV absorption band at ~330 nm. In other word, the blue emission is attributed to electronic states created by the aggregation of BPD, and the green emission arises from LUMO to HOMO transitions. BPD shows a substantial decrease in PL intensity with increase in concentration in DCM. The PLQY of BPD measured at different concentrations is shown in Figure 1c. Dilute solutions of ~2 µg/mL have a high PLQY of 27.7 %; however, PLQY decreases significantly to 2.5 % when concentration is increased to 1000 µg/mL (0.075 wt. %). This drastic decrease in PLQY is attributed to concentration quenching, reabsorption, and aggregation. The occurrence of blue PL emission due to aggregation in addition to the green emission caused by LUMO to HOMO transition makes the PL emission spectrum very broad, which is very useful for the application of BPD in white light-emitting devices (LEDs).

In particular, the strong PL emission suggests that BPD can be a suitable candidate for application in CCL in optically driven LEDs. At the same time, its aromatic structure (as shown in **Figure 2a)** indicates that BPD may have electrical properties that may be useful in the active layer of electrically driven LEDs. Therefore, the optical properties of BPD were first investigated in different insulating polymers (PMMA, PS, and optical epoxy) and a semiconducting polymer (PVK) that is widely used as a host material in the active layer of organic LEDs. The molecular structures of PMMA, PS, and PVK are shown in Figure 2b, c, and d, respectively**.** BPD was mixed in these polymers at concentrations of 0.10, 0.25, 0.50, 0.75, 1.00, and 2.00 wt. % and films were fabricated (see Experimental section for the details). Optical photographs of the films were taken with a fluorescence microscope using a 365 nm excitation wavelength (Figure 2e-h). It can be seen from the images that the PL emission color of the films changes with concentration. For epoxy, PMMA, and PVK films, there is a redshift in PL emission color with increasing concentration of BPD that is attributed to increased reabsorption of shorter wavelength emission. However, in PS, the PL emission color of the films shows a blue shift with increasing BPD concentration. This is due to the fact that, in PS, BPD tends to aggregate more than in the other polymers. This is evident from the UV-vis absorbance spectra of BPD measured in all polymer matrices; see **Figure 3a**. The peak at 510 nm that is assigned to monomer absorption of BPD is reduced and appears redshifted in PS. The apparent redshift in the monomer absorption may be due to chemical interaction with the PS. The overall high baseline absorbance may be attributed to the scattering from the aggregates. The diminished monomer absorption confirms that the aggregation of BPD is much higher in PS, even at lower concentrations compared to the other polymers. Therefore, BPD shows a lower degree of reabsorption of blue emission due to lower absorption at longer wavelengths in PS. On the other hand, as concentration increases, the aggregation increases as well, which causes the enhancement of blue emission, i.e., emission from aggregation states. That is the reason a blue shift in PL emission color is observed in PS, while a redshift is observed in all other polymers.

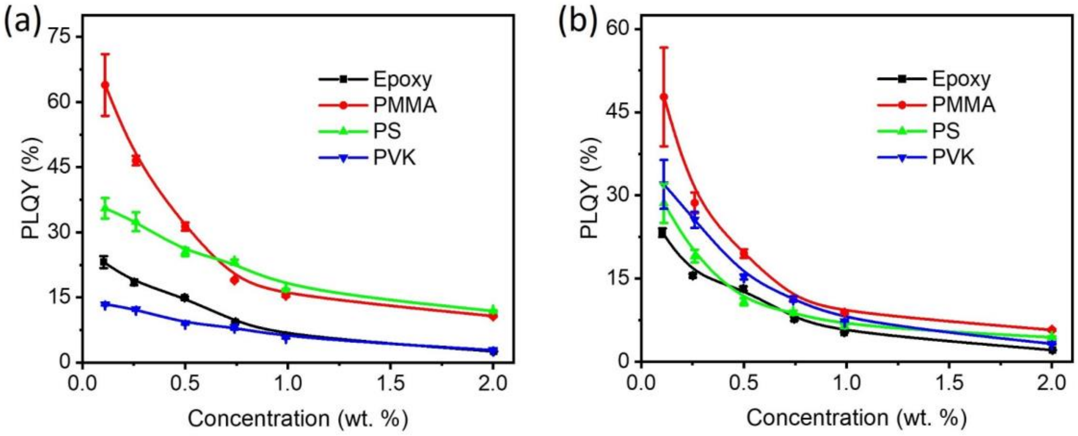

Figure 4: PLQY of BPD mixed in different polymers at different concentration measured using excitation wavelengths of (a) 340* nm, (b) 375 nm. Error bars show the standard deviation in the measurements. *PLQY in PVK was measured using an excitation wavelength of 353 nm, instead of 340 nm, due to the high absorption of PVK at shorter wavelengths.

Reabsorption of short wavelength emission and the shifts in the PL emission color can also be seen in the PL emission spectra of BPD measured in different polymers; see Figure 2i-l and Figure S1-S4 in the Electronic Supplementary Information (ESI). PL emission spectra of BPD in epoxy and PMMA show three distinct features: first, in the blue wavelength range; second, the most intense one, in green wavelength range; and third, in the yellow region that makes the spectrum broad. It can be seen that the PL emission intensity of the long wavelength (yellow) emission increases with respect to short wavelength emission with increasing concentration of BPD; this is due to the reabsorption of blue and green PL emission that causes the noticeable change in color of the films. In PVK, an additional PL emission peak is observed at 425 nm due to PL emission from PVK that becomes prominent when the concentration of BPD is low. Apart from that, concentration-dependent PL emission spectra show a similar relative increase in long wavelength emission due to reabsorption. However, in PS, the relative PL intensity of short wavelength (blue) emission increases with concentration; see Figure 2c. As discussed above, there is little absorption from BPD monomers (at 477 nm and 510 nm); therefore, blue PL emission arising from aggregation states is not reabsorbed, while increasing concentration causes an increase in aggregation and, hence, the intensity of blue PL emission increases with concentration.[11]

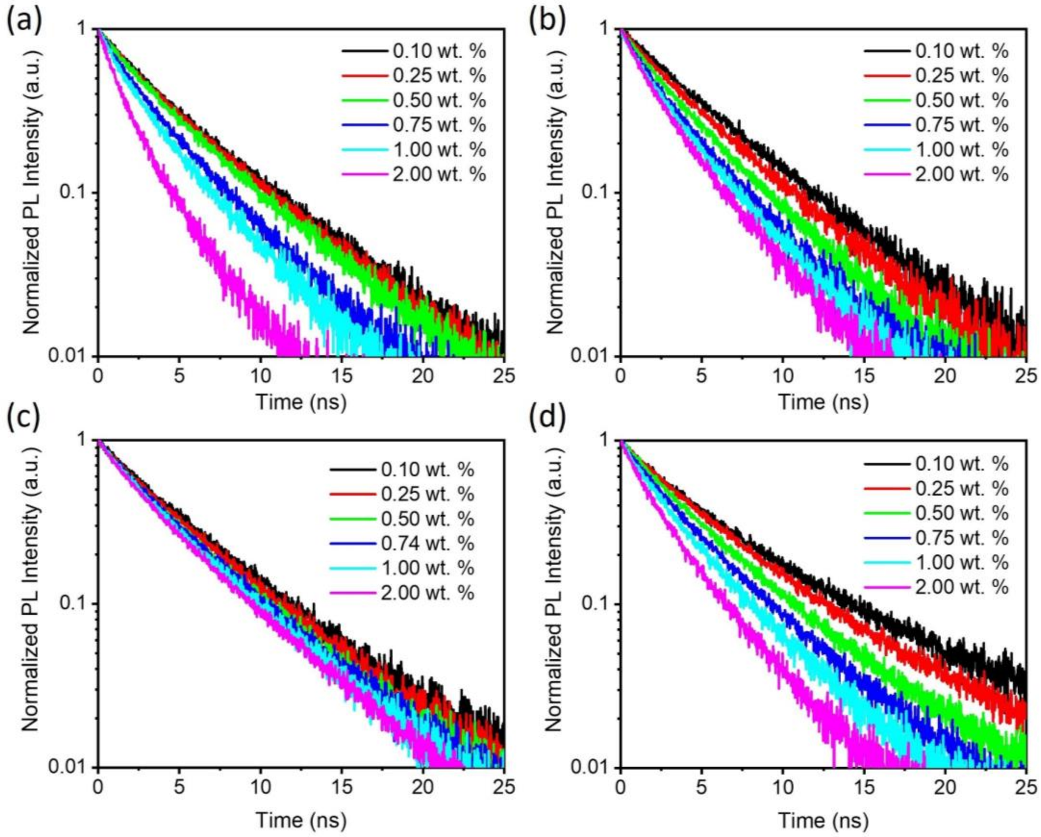

Figure 5: PL lifetime spectra of BPD mixed in (a) Epoxy, (b) PMMA, (c) PS, and (d) PVK at different concentration recorded using an excitation wavelength of 375 nm.

PLQY measurements of BPD in all polymers show a strong concentration dependence in the solid state as well. At low concentrations, the PLQY is high and sharply drops with increasing concentration of BPD. The optimum excitation wavelength for measurement of PLQY is ~340 nm (Figure 1a). The average PLQY of 0.1 wt. % of BPD in PMMA measured using an excitation wavelength of 340 nm is 64 % with a standard deviation of 7.1 % (**Figure 4a**). The highest measured value of 0.1 wt. % samples is 75.9 %, and it drops to ~11 % when concentration increases to 2.0 wt. %. Higher PLQY in solid matrices than in solutions is common in the literature that is usually attributed to the more confined and rigid environment in solid.[22, 23] Similarly, the PLQY in PS varies from 35.5 % to ~11%. Again, the lower PLQY in PS is attributed to aggregation and a lack of PL emission from monomers. On the other hand, PLQY values of BPD measured in epoxy and PVK are 23.2 % and 13.5 %. This significant difference is due to the high absorption of epoxy and PVK at short wavelength regions; see Figure 3b. This high background absorption of epoxy and PVK results in lower PLQY values. To overcome this issue, PLQY was also measured using 375 nm excitation (Figure 4b). The PLQY values exhibit similar decreases with increasing

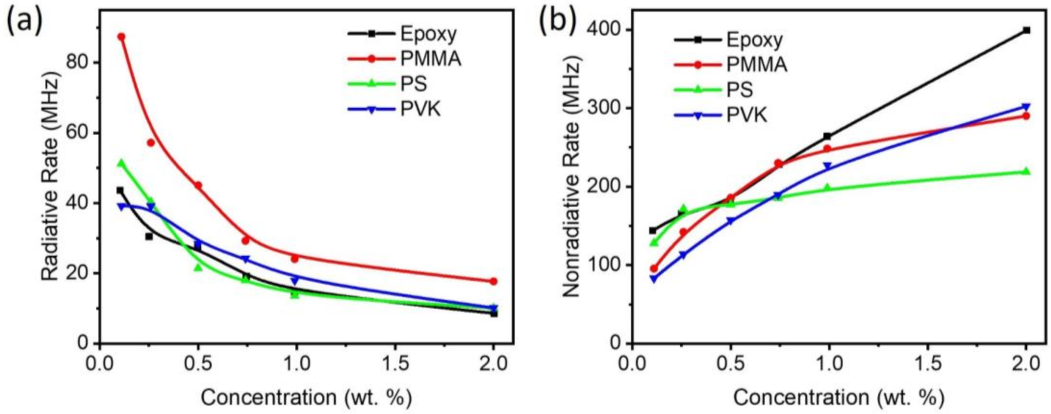

Figure 6: (a) Radiative rate and (b) nonradiative rate of BPD vs. concentration in epoxy, PMMA, PS, and PVK calculated from the PLQY and lifetime measurements.

concentration; however, the average PLQY is slightly lower than that measured using 340 nm excitation. This is due to the less efficient excitation of BPD at this wavelength (see Figure 1a). However, the spread in the PLQY values measured in different polymer matrices is lower due to less background absorption from PVK and epoxy than that observed with 340 nm excitation. The slight variation in PLQY values across different polymers may be attributed to differences in the rigidity of matrices and the interaction of BPD with the matrices.

Time-resolved photoluminescence (TRPL) of the films was measured using a 375 nm excitation wavelength, and the emission was collected using a 400 nm long pass filter (see **Figure 5**). The measured data was fitted with a double-exponential decay function. Typically, the average lifetime of the films varies between ~2.5 ns to ~5.6 ns; however, in PVK, the lifetime values are slightly longer (e.g., 8.2 ns for the 0.1 wt. % sample) due to contributions from PVK emission to the lifetime. It is important to mention here that PVK is a wide bandgap semiconductor that emits weakly in the blue wavelength region at ~450 nm. Its PL lifetime is 15.6 ns, which affects the PL lifetime measurements for BPD, especially at lower concentrations. The PL lifetime decreases with increasing concentration of BPD in all polymer matrices. For instance, the average PL lifetime of BPD in epoxy is 5.3 ns at 0.1 wt. % concentration of BPD, and it decreases to 1.5 ns when the concentration is increased to 2.0 wt. %. In PS, the shortening of the PL lifetime is not significant; this can be attributed to the low solubility of BPD in PS, which can cause aggregation at even lower concentrations. As it has been noted above, a strong reabsorption is observed in the BPD films that increases with increasing concentration. It is well known that reabsorption can lengthen the PL lifetime of fluorophores.[30, 31] Contrary to the literature, a shortening of the PL lifetime was observed with increasing concentration (or reabsorption). This confirms that there is another phenomenon that plays an important role in decreasing quantum yield. We attribute this shortening of lifetime to nonradiative recombination pathways that form by aggregation of molecules that dominates over the effects of reabsorption. Furthermore, the PL lifetime has two components: τ_1 is assigned to PL emission from the monomers because its value is close to that measured in solution,[11] and τ_2 is attributed to PL emission from the states formed by aggregation of BPD. The intensities of lifetime components A_1 and A_2 are given in **Table 1**. The contribution of monomers to TRPL intensity (A_1) decreases, and that of aggregates (A_2) increases with increasing concentration. This further confirms the aggregation of BPD at high concentrations. In PVK, A_1 and A_2 change differently; it appears that the contribution from aggregates (A_2) decreases with increasing concentration. This behavior is attributed to a contribution of PVK emission to the total PL emission in lifetime measurements.

The decrease in PL lifetime and PLQY with the increasing concentration of BPD suggest increases in nonradiative rates. Radiative and nonradiative rates are calculated from PLQY and PL lifetime measurements; see **Figure 6** and Table 1. The variation in radiative rates with concentration is similar to PLQY; however, nonradiative rates increase significantly with increasing concentration. This further confirms that the shortening of PL lifetime is due to nonradiative decay pathways that form by aggregation.

Table 1: Radiative and nonradiative rates of BPD in different polymers calculated from PLQY and PL lifetime measured using 375 nm excitation.

Polymer Matrix	Concentration (wt. %)	PLQY (%)	τ_1 (ns)	A_1 (%)	τ_2 (ns)	A_2 (%)	τ_{av} (ns)	Γ_{red} (MHz)	Γ_{nrad} (MHz)
Epoxy	0.1	23.3	6.3	54.8	2.7	45.2	5.3	43.7	143.9
	0.25	15.5	6.0	55.4	2.5	44.6	5.1	30.5	165.9
	0.5	13.2	5.6	56.1	2.4	43.9	4.8	27.5	180.2
	0.75	7.7	5.0	47.6	2.0	52.4	4.0	19.1	228.2
	1.0	5.3	4.6	42.5	1.8	57.5	3.6	14.8	264.0
	2.0	2.1	3.5	29.1	1.2	70.9	2.4	8.6	399.2
PMMA	0.1	47.7	6.2	63.0	3.1	37.0	5.5	87.4	95.7
	0.25	28.7	5.7	60.3	2.7	39.7	5.0	57.2	142.3
	0.5	19.5	5.1	55.3	2.2	44.7	4.3	45.1	185.9
	0.75	11.3	4.7	48.0	2.0	52.0	3.8	29.3	230.2
	1.0	8.8	4.7	42.3	1.9	57.7	3.7	24.1	248.4
	2.0	5.8	4.2	40.1	1.7	59.9	3.3	17.7	290.1
PS	0.1	28.6	6.5	58.1	3.1	41.9	5.6	51.2	127.9
	0.25	19.1	6.2	39.9	3.0	60.1	4.7	40.4	171.6
	0.5	10.8	5.8	58.0	2.7	42.0	5.0	21.5	177.1
	0.75	8.9	5.6	59.5	2.6	40.5	4.9	18.0	185.5
	1.0	6.4	5.5	58.1	2.4	41.9	4.7	13.6	198.0
	2.0	4.4	5.3	48.5	2.3	51.6	4.4	10.1	218.7
PVK	0.1	32.0	12.6	23.0	4.2	77.0	8.2	39.2	83.2
	0.25	25.6	10.2	21.3	4.0	78.7	6.5	39.1	113.8
	0.5	15.3	7.7	27.8	3.4	72.2	5.4	28.5	157.4
	0.75	11.4	6.3	33.7	2.8	66.3	4.7	24.3	189.5
	1.0	7.3	5.7	29.3	2.5	70.7	4.1	18.0	227.7
	2.0	3.3	4.5	30.8	1.8	69.2	3.2	10.2	302.3

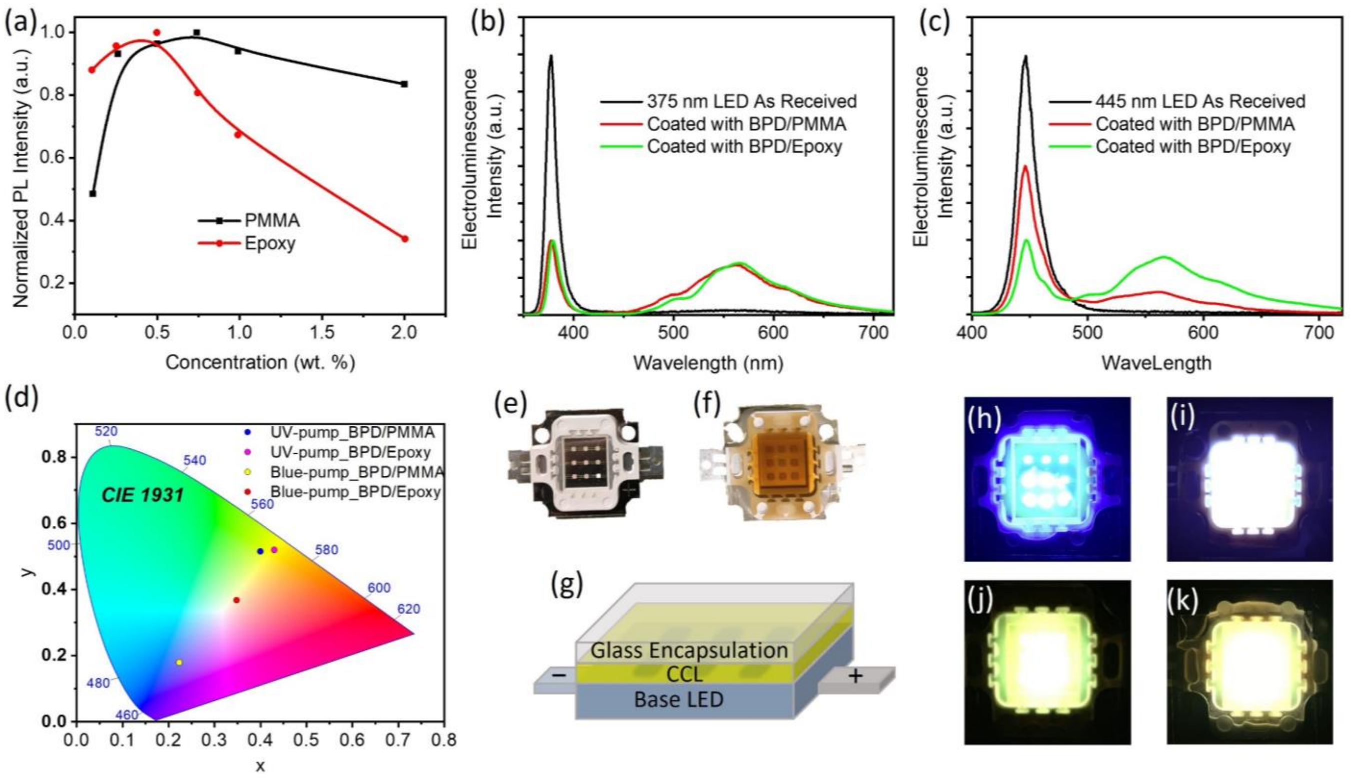

Figure 7: (a) The normalized PL intensity of BPD in PMMA and epoxy vs. concentration. Electroluminescence of LEDs fabricated (b) using UV (375 nm) pump and (c) using blue (445 nm) pump. (d) CIE 1931 xy chromaticity space showing the color coordinates of the LEDs, calculated from the spectra given in (b) and (c). Optical photograph of an LED (e) before applying color converting layer (CCL) and (f) after applying CCL. (g) Schematic representation of the device structure. Optical photograph of (h) blue-pumped LED with BPD/PMMA as CCL, (i) blue-pumped LED with BPD/Epoxy as CCL, (j) UV-pumped LED with BPD/Epoxy as CCL, and (k) UV-pumped LED with BPD/PMMA as CCL.

The observed optical properties provide an insight into the morphology of the aggregates. Commonly found aggregation structures of π-conjugated molecules (such as BPD) include X-, J- and H aggregates. Usually, J- and X-aggregates are identified by a redshift in optical absorption spectra and an increase in PLQY.[32-35] On the other hand, the characteristic features of H-aggregates include blueshifts (compared with the monomers) in optical absorption spectra, fluorescence quenching and lower radiative decay rates.[36] Therefore, it is likely that BPD aggregates have H-type structure. So, it is inferred that as the concentration of BPD increases in the polymers, the concentration of H-aggregates increases that consequently causes the fluorescence quenching and the reduction in radiative decay rates.

For the application of BPD in the CCL of optically pumped LEDs, first, the optimum concentration was determined. As mentioned above, at lower concentration, the PLQY of BPD is higher, but for optimum performance, the CCL should have a higher absorption so that it can convert a significant portion of the pump light to the visible region. Higher absorption can be achieved by increasing the concentration of BPD in the polymer matrices; however, increasing concentration decreases the PLQY. To determine the optimum concentration, the integrated PL emission of the films was plotted versus concentration (**Figure 7a**), and it was found that films made of 0.5 wt. % concentration had the highest PL emission intensity. Therefore, the devices were fabricated using this concentration value. Figure 7b shows the electroluminescence spectra of the UV-pumped (375 nm) LEDs before and after the application of the CCL. The UV-pumped LEDs show a broad spectrum centered around the yellow wavelength region (500-650 nm) in addition to the sharp peak due to the base LED. CIE 1931 color coordinates of the UV-pumped LEDs coated with BPD/epoxy and BPD/PMMA CCLs are (0.43, 0.52) and (0.40, 0.51), respectively, which lie in the yellow color region (see Figure 7j). The luminous efficiency of these LEDs measured at a driving voltage of 10 V is 1.4 lm/W (luminance 24,368 cd/m^2) and 1.9 lm/W (luminance 33,297 cd/m^2), respectively. The electroluminescence color of BPD appears redshifted compared with the PL emission. This is because PL is measured from the front face of the thin films. On the other hand, the CCL is excited from the bottom, and the emission is collected from the top. This, combined with the higher thickness of CCL, increases the reabsorption of shorter wavelengths and, hence, causes the redshift in the apparent emission color of BPD.[26] To take advantage of this phenomenon, white-emitting LEDs were fabricated using a blue pump (445 nm). Electroluminescence spectra of blue-pumped LEDs are shown in Figure 7c. LEDs fabricated using BPD/epoxy as CCL show almost pure white emission color (color rendering index (CRI): 71) with CIE 1931 color coordinates of (0.35, 0.37) (see Figure 7d and i) and luminous efficiency of 3.8 lm/W (luminance 43,331 cd/m^2) at a driving voltage of 10 V. In terms of luminance, the values achieved in this study are significantly higher than the values reported in the literature on CD-based white LEDs.[21] The luminous efficiency value of the white LEDs in this work is comparable with CD-based single-component white LEDs (without mixing CDs of multiple colors[37-39] or CDs with conventional rare-earth element-based phosphors[40-42]) reported in the literature; see Table S1 in the ESI.[43]

Conclusions

Detailed optical characterization of N^4,N^{11}-dimethyldibenzo[a,h]phenazine-4,11-diamine (BPD) – a molecular fluorophore that forms carbon dots – in the solid state has been carried out. A high PLQY value (75.9 %) from BPD in a PMMA matrix was recorded. The PLQY of BPD in other solid matrices was also investigated. It was observed that the PLQY of BPD films decreased significantly with increasing concentration of BPD in the solid matrices. Along with the reduction in PLQY, a considerable redshift in PL emission color and a shortening of PL lifetime were also observed. Based on these observations, it was concluded that the PLQY decreased due to reabsorption by BPD itself and nonradiative pathways created by aggregation at higher concentration. Furthermore, optically driven LEDs were fabricated having a different emission color that depends on the pump wavelength and the thickness and matrix of the CCL. UV-pumped LEDs having yellow color were fabricated with luminous efficiency up to 1.9 lm/W. Fabrication of LEDs with almost pure white emission color having CIE coordinates of (0.35, 0.37) using a blue pump has also been demonstrated. Blue-pumped white LEDs show a luminous efficiency of 3.8 lm/W for BPD at a concentration of 0.5 wt. % in an epoxy matrix.

Author Contributions

N. J. conceived, designed, and carried out the experiments, analyzed the results and prepared the manuscripts. H.P., S.S., J. C., and Z. C. helped in sample preparation, results analysis, and manuscript writing. D. O. conceived, designed, and supervised the project.

Conflicts of interest

There are no conflicts to declare.

Acknowledgements

This work was supported in part by funding from the U. S. National Science Foundation, grant DMR-1554954. N. J. acknowledges funding from the Fulbright scholarship program.

References

1. K. J. Mintz, Y. Zhou and R. M. Leblanc, Recent development of carbon quantum dots regarding their optical properties, photoluminescence mechanism, and core structure, *Nanoscale*, 2019, **11**, 4634-4652.
2. N. Javed and D. M. O'Carroll, Carbon Dots and Stability of Their Optical Properties, *Particle & Particle Systems Characterization*, 2021, **38**, 2000271.
3. B. Zhao, H. Ma, M. Zheng, K. Xu, C. Zou, S. Qu and Z. a. Tan, Narrow-bandwidth emissive carbon dots: A rising star in the fluorescent material family, *Carbon Energy*, 2022, **4**, 88-114.
4. B. Wang, G. I. N. Waterhouse and S. Lu, Carbon dots: mysterious past, vibrant present, and expansive future, *Trends in Chemistry*, 2023, **5**, 76-87.
5. D. Qu and Z. Sun, The formation mechanism and fluorophores of carbon dots synthesized via a bottom-up route, *Materials Chemistry Frontiers*, 2020, **4**, 400-420.
6. A. Sharma and J. Das, Small molecules derived carbon dots: synthesis and applications in sensing, catalysis, imaging, and biomedicine, *Journal of Nanobiotechnology*, 2019, **17**, 92.
7. S. Zhu, X. Zhao, Y. Song, S. Lu and B. Yang, Beyond bottom-up carbon nanodots: Citric-acid derived organic molecules, *Nano Today*, 2016, **11**, 128-132.
8. Y. Song, S. Zhu, S. Zhang, Y. Fu, L. Wang, X. Zhao and B. Yang, Investigation from chemical structure to photoluminescent mechanism: a type of carbon dots from the pyrolysis of citric acid and an amine, *Journal of Materials Chemistry C*, 2015, **3**, 5976-5984.
9. L. Shi, J. H. Yang, H. B. Zeng, Y. M. Chen, S. C. Yang, C. Wu, H. Zeng, O. Yoshihito and Q. Zhang, Carbon dots with high fluorescence quantum yield: the fluorescence originates from organic fluorophores, *Nanoscale*, 2016, **8**, 14374-14378.
10. B. Wang and S. Lu, The light of carbon dots: From mechanism to applications, *Matter*, 2022, **5**, 110-149.
11. N. Javed, Z. Cheng, K. Zhu, R. Crichton, H. Maddali, G. Hall, J. Zhang, J. Li and D. M. O’Carroll, Carbon Dot-like Molecular Nanoparticles, Their Photophysical Properties, and Implications for LEDs, *ACS Applied Nano Materials*, 2022, **5**, 11741-11751.
12. N. Javed and D. M. O'Carroll, Long-term effects of impurities on the particle size and optical emission of carbon dots, *Nanoscale Advances*, 2021, **3**, 182-189.
13. J. Shao, S. Zhu, H. Liu, Y. Song, S. Tao and B. Yang, Full-Color Emission Polymer Carbon Dots with Quench-Resistant Solid-State Fluorescence, *Advanced Science*, 2017, **4**, 1700395.
14. H. Yang, Y. Liu, Z. Guo, B. Lei, J. Zhuang, X. Zhang, Z. Liu and C. Hu, Hydrophobic carbon dots with blue dispersed emission and red aggregation-induced emission, *Nature Communications*, 2019, **10**, 1789.
15. V. Gude, A. Das, T. Chatterjee and P. K. Mandal, Molecular origin of photoluminescence of carbon dots: aggregation-induced orange-red emission, *Physical Chemistry Chemical Physics*, 2016, **18**, 28274-28280.
16. P. Ma, X. Sun, W. Pan, G. Yu and J. Wang, Green and Orange Emissive Carbon Dots with High Quantum Yields Dispersed in Matrices for Phosphor-Based White LEDs, *ACS Sustainable Chemistry & Engineering*, 2020, **8**, 3151-3161.
17. F. Yuan, Y.-K. Wang, G. Sharma, Y. Dong, X. Zheng, P. Li, A. Johnston, G. Bappi, J. Z. Fan, H. Kung, B. Chen, M. I. Saidaminov, K. Singh, O. Voznyy, O. M. Bakr, Z.-H. Lu and

E. H. Sargent, Bright high-colour-purity deep-blue carbon dot light-emitting diodes via efficient edge amination, *Nature Photonics*, 2020, **14**, 171-176.

18. B. Zhao and Z. a. Tan, Fluorescent Carbon Dots: Fantastic Electroluminescent Materials for Light-Emitting Diodes, *Advanced Science*, 2021, **8**, 2001977.
19. H. Jia, H. Ma, X. Liu, D. Xu, T. Yuan, C. Zou and Z. a. Tan, Engineering organic–inorganic perovskite planar heterojunction for efficient carbon dots based light-emitting diodes, *Applied Physics Reviews*, 2022, **9**.
20. J. Ren, L. Stagi and P. Innocenzi, Fluorescent carbon dots in solid-state: From nanostructures to functional devices, *Progress in Solid State Chemistry*, 2021, **62**, 100295.
21. T. Feng, Q. Zeng, S. Lu, X. Yan, J. Liu, S. Tao, M. Yang and B. Yang, Color-Tunable Carbon Dots Possessing Solid-State Emission for Full-Color Light-Emitting Diodes Applications, *ACS Photonics*, 2018, **5**, 502-510.
22. Y. Liu, P. Wang, K. A. Shiral Fernando, G. E. LeCroy, H. Maimaiti, B. A. Harruff-Miller, W. K. Lewis, C. E. Bunker, Z.-L. Hou and Y.-P. Sun, Enhanced fluorescence properties of carbon dots in polymer films, *Journal of Materials Chemistry C*, 2016, **4**, 6967-6974.
23. J. Guo, Y. Lu, A.-Q. Xie, G. Li, Z.-B. Liang, C.-F. Wang, X. Yang and S. Chen, Yellow-Emissive Carbon Dots with High Solid-State Photoluminescence, *Advanced Functional Materials*, 2022, **32**, 2110393.
24. R. Fu, H. Song, X. Liu, Y. Zhang, G. Xiao, B. Zou, G. I. N. Waterhouse and S. Lu, Disulfide Crosslinking-Induced Aggregation: Towards Solid-State Fluorescent Carbon Dots with Vastly Different Emission Colors†, *Chinese Journal of Chemistry*, 2023, **41**, 1007-1014.
25. J. Ren, J. Sun, X. Sun, R. Song, Z. Xie and S. Zhou, Precisely Controlled Up/Down-Conversion Liquid and Solid State Photoluminescence of Carbon Dots, *Advanced Optical Materials*, 2018, **6**, 1800115.
26. Y. Wang, S. Kalytchuk, Y. Zhang, H. Shi, S. V. Kershaw and A. L. Rogach, Thickness-Dependent Full-Color Emission Tunability in a Flexible Carbon Dot Ionogel, *The Journal of Physical Chemistry Letters*, 2014, **5**, 1412-1420.
27. X. Meng, Q. Chang, C. Xue, J. Yang and S. Hu, Full-colour carbon dots: from energy-efficient synthesis to concentration-dependent photoluminescence properties, *Chemical Communications*, 2017, **53**, 3074-3077.
28. Y. Xiong, J. Schneider, E. V. Ushakova and A. L. Rogach, Influence of molecular fluorophores on the research field of chemically synthesized carbon dots, *Nano Today*, 2018, **23**, 124-139.
29. K. Smet, J. Schanda, L. A. Whitehead and R. Luo, CRI2012: A proposal for updating the CIE colour rendering index, *Lighting Research & Technology*, 2013, **45**, 689 - 709.
30. F. Staub, H. Hempel, J.-C. Hebig, J. Mock, U. W. Paetzold, U. Rau, T. Unold and T. Kirchartz, Beyond Bulk Lifetimes: Insights into Lead Halide Perovskite Films from Time-Resolved Photoluminescence, *Physical Review Applied*, 2016, **6**, 044017.
31. H. Diab, C. Arnold, F. Lédée, G. Trippé-Allard, G. Delport, C. Vilar, F. Bretenaker, J. Barjon, J.-S. Lauret, E. Deleporte and D. Garrot, Impact of Reabsorption on the Emission Spectra and Recombination Dynamics of Hybrid Perovskite Single Crystals, *The Journal of Physical Chemistry Letters*, 2017, **8**, 2977-2983.
32. F. Würthner, T. E. Kaiser and C. R. Saha-Möller, J-Aggregates: From Serendipitous Discovery to Supramolecular Engineering of Functional Dye Materials, *Angewandte Chemie International Edition*, 2011, **50**, 3376-3410.
33. N. J. Hestand and F. C. Spano, Expanded Theory of H- and J-Molecular Aggregates: The Effects of Vibronic Coupling and Intermolecular Charge Transfer, *Chemical Reviews*, 2018, **118**, 7069-7163.
34. S. Ma, Y. Liu, J. Zhang, B. Xu and W. Tian, Polymorphism-Dependent Enhanced Emission in Molecular Aggregates: J-Aggregate versus X-Aggregate, *The Journal of Physical Chemistry Letters*, 2020, **11**, 10504-10510.
35. A. V. Sorokin, I. Y. Ropakova, R. S. Grynyov, M. M. Vilkisky, V. M. Liakh, I. A. Borovoy, S. L. Yefimova and Y. V. Malyukin, Strong difference between optical properties and morphologies for J-Aggregates of similar cyanine dyes, *Dyes and Pigments*, 2018, **152**, 49-53.
36. S. Ma, S. Du, G. Pan, S. Dai, B. Xu and W. Tian, Organic molecular aggregates: From aggregation structure to emission property, *Aggregate*, 2021, **2**, e96.
37. R. Kumari, A. Kumar, K. Negi and S. K. Sahu, Multicolor-Emissive Carbon Dots for White-Light-Emitting Diodes and Room-Temperature Phosphorescence, *ACS Applied Nano Materials*, 2023, **6**, 918-929.
38. Z. Yan, T. Chen, L. Yan, X. Liu, J. Zheng, F.-d. Ren, Y. Yang, B. Liu, X. Liu and B. Xu, One-Step Synthesis of White-Light-Emitting Carbon Dots for White LEDs with a High Color Rendering Index of 97, *Advanced Science*, 2023, **10**, 2206386.
39. T. Hu, Z. Wen, C. Wang, T. Thomas, C. Wang, Q. Song and M. Yang, Temperature-controlled spectral tuning of full-color carbon dots and their strongly fluorescent solid-state polymer composites for light-emitting diodes, *Nanoscale Advances*, 2019, **1**, 1413-1420.
40. D. Chen, H. Gao, X. Chen, G. Fang, S. Yuan and Y. Yuan, Excitation-Independent Dual-Color Carbon Dots: Surface-State Controlling and Solid-State Lighting, *ACS Photonics*, 2017, **4**, 2352-2358.
41. X. Zhang, H. Yang, Z. Wan, T. Su, X. Zhang, J. Zhuang, B. Lei, Y. Liu and C. Hu, Self-Quenching-Resistant Red Emissive Carbon Dots with High Stability for Warm White Light-Emitting Diodes with a High Color Rendering Index, *Advanced Optical Materials*, 2020, **8**, 2000251.
42. M. Wu, J. Zhan, B. Geng, P. He, K. Wu, L. Wang, G. Xu, Z. Li, L. Yin and D. Pan, Scalable synthesis of organic-soluble carbon quantum dots: superior optical properties in solvents, solids, and LEDs, *Nanoscale*, 2017, **9**, 13195-13202.
43. C. Ji, W. Xu, Q. Han, T. Zhao, J. Deng and Z. Peng, Light of carbon: Recent advancements of carbon dots for LEDs, *Nano Energy*, 2023, **114**, 108623.